Eur. Phys. J. A **26**, 301–305 (2005)
DOI 10.1140/epja/i2005-10175-2

THE EUROPEAN PHYSICAL JOURNAL A

First direct measurement of the total cross-section of $^{12}C(\alpha,\gamma)^{16}O$

D. Schürmann[1], A. Di Leva[1], L. Gialanella[2], D. Rogalla[3], F. Strieder[1,a], N. De Cesare[4], A. D'Onofrio[3], G. Imbriani[2], R. Kunz[1], C. Lubritto[3], A. Ordine[2], V. Roca[2], C. Rolfs[1], M. Romano[2], F. Schümann[1], F. Terrasi[3], and H.-P. Trautvetter[1]

[1] Institut für Experimentalphysik III, Ruhr-Universität Bochum, Bochum, Germany
[2] Dipartimento di Scienze Fisiche, Università Federico II, Napoli and INFN, Napoli, Italy
[3] Dipartimento di Scienze Ambientali, Seconda Università di Napoli, Caserta and INFN, Napoli, Italy
[4] Dipartimento di Scienze della Vita, Seconda Università di Napoli, Caserta and INFN, Napoli, Italy

Received: 29 September 2005 / Revised version: 17 November 2005 /
Published online: 29 November 2005 –
Communicated by R. Krücken

Abstract. The total cross-section of $^{12}C(\alpha,\gamma)^{16}O$ was measured for the first time by a direct and ungated detection of the ^{16}O recoils. This measurement in inverse kinematics using the recoil mass separator ERNA in combination with a windowless He gas target allowed to collect data with high precision in the energy range $E = 1.9$ to 4.9 MeV. The data represent new information for the determination of the astrophysical $S(E)$ factor.

PACS. 25.55.-e ^{3}H-, ^{3}He-, and ^{4}He-induced reactions – 26.20.+f Hydrostatic stellar nucleosynthesis

1 Introduction

The radiative capture reaction $^{12}C(\alpha,\gamma)^{16}O$ (Q = 7.16 MeV) takes place during stellar core helium burning [1], where ^{12}C is produced by the triple-alpha process. The capture cross-section $\sigma(E_0)$ at the relevant Gamow energy, $E_0 \approx 0.3$ MeV for $T \approx 2 \times 10^8$ K, determines —together with the convection mechanism at the edge of the stellar core [2]— the abundances of carbon and oxygen at the end of helium burning. This, in turn, strongly influences the nucleosynthesis of elements up to the iron region for massive stars [2] and the composition of CO white dwarfs, whose progenitors are intermediate- and low-mass stars [3].

A recent experiment confirmed that the reaction rate of the triple-alpha process is known with a precision of about 10% for temperatures near 10^8 K [4]. A similar precision is needed for the rate of $^{12}C(\alpha,\gamma)^{16}O$ to provide an adequate input for stellar models [5]. The remarkable experimental efforts over the last decades [6–14] focused on the observation of the capture γ-rays, including one experiment [9] that used the coincident detection of the ^{16}O recoils. Due to the low cross-section and various background sources depending on the exact nature of the experiments, γ-ray data with useful but still inadequate precision were limited to center-of-mass energies $E_{cm} = E = 1.0$ to 3.2 MeV. At the low-energy range, the data were limited *e.g.* by cosmic-ray background and at the high-energy range the data were limited by intense background reactions such as $^{13}C(\alpha,n)^{16}O$ (for an α-beam experiment) and $^{12}C(^{12}C,n)^{23}Mg$ (for a ^{12}C beam experiment).

The cross-section $\sigma(E_0)$ is expected to be dominated by p-wave ($E1$) and d-wave ($E2$) capture to the ($J^\pi = 0^+$) ^{16}O ground state. Two bound states, at 6.92 MeV ($J^\pi = 2^+$) and 7.12 MeV ($J^\pi = 1^-$), which correspond to subthreshold resonances at $E_R = -245$ and -45 keV, appear to provide the bulk of the capture strength $\sigma(E_0)$ through their finite widths that extend into the continuum. R-matrix analyses are performed, in order to model the energy dependence of the cross-section. In these analyses the contribution of each amplitude to the total cross-section is expressed in terms of a small number of resonances and a direct capture contribution. The parameters of the model are determined by a fit to the experimental data. The extrapolation to $E_0 = 0.3$ MeV is sensitive to the properties of the nearby levels, but it is sensitive also to the properties of the high-lying resonances, since their tails extend to low energy. The effect of these resonances is usually included by a single high-energy "background" resonance —one for each amplitude; these resonances are needed to obtain a good fit to the data.

Analyses of the available capture data together with data from the α-^{12}C elastic scattering and the β-delayed

[a] e-mail: strieder@ep3.rub.de

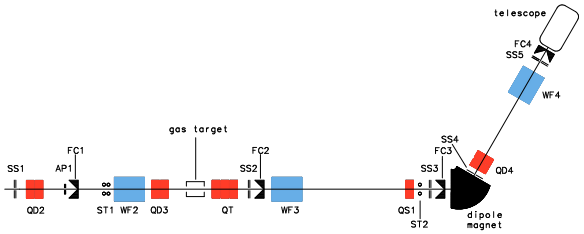

Fig. 1. Schematic diagram of the recoil separator ERNA. WF = Wien filter, QS = quadrupole singlet, QD = quadrupole doublet, QT = quadrupole triplet, ST = steerer, FC = Faraday cup, SS = slit system, AP = aperture. At the end of the separator, there is a ΔE-E telescope for particle identification.

α-decay of ^{16}N still lead to large uncertainties in the extrapolation to E_0 [15]. This is partly caused by large errors, both statistical and systematic, affecting the low-energy capture data, and partly due to the weak experimental constraints of the background resonances. Clearly, new measurements at low energies are needed. However, of equal importance are also new measurements at significantly higher energies, well above the range of the recent experiments, which may improve the experimental characterization of the background resonances and may thus reduce the uncertainty in the extrapolated astrophysical S factor $S(E_0)$. There may exist even an s-wave capture (monopole $E0$) and significant capture amplitudes to excited ^{16}O states. Since the various capture amplitudes have different energy dependences, a better knowledge of the individual amplitudes requires new data at both low and high energies to provide an improved basis for their extrapolation to E_0.

2 Equipment and setup

A new experimental approach (fig. 1) has been developed at the 4 MV Dynamitron tandem accelerator in Bochum, called ERNA = European Recoil separator for Nuclear Astrophysics [16–20]. In this approach, the reaction is initiated in inverse kinematics, ^{4}He(^{12}C, γ)^{16}O, *i.e.* a ^{12}C ion beam with a particle current of up to 10 μA is guided into a windowless ^{4}He gas target. A beam contamination in the order of 6×10^{-10} ^{16}O ions per incident ^{12}C projectile was found, by far too high for a direct detection of the ^{16}O recoils. Therefore, for the purpose of beam purification, there is one Wien filter before the analysing magnet (WF1, not shown in fig. 1) and one before the gas target (WF2); with this combination a beam purity better than 10^{-18} could be achieved [16]. The windowless gas target —entrance and exit aperture of the gas cell with a diameter of 6 mm— includes an Ar post-target stripping system. After the gas target, the separator consists sequentially of the following elements: a quadrupole triplet (QT), a Wien filter (WF3), a quadrupole singlet (QS), a 60° dipole magnet, a quadrupole doublet (QD4), and a Wien filter (WF4). The recoil separator suppresses the intense ^{12}C beam; the ^{16}O recoils in a selected charge state

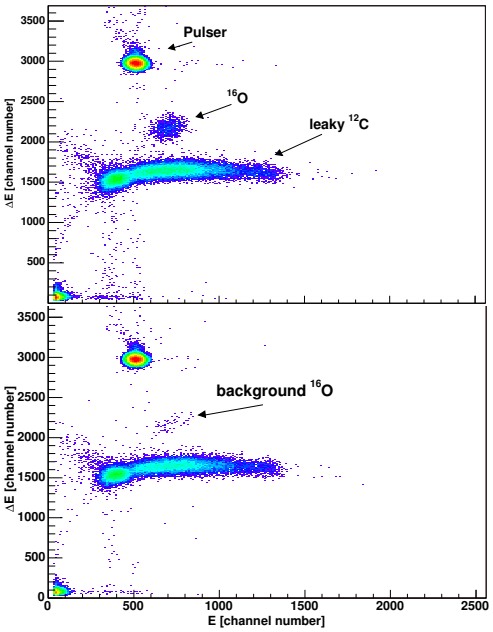

Fig. 2. Identification matrix of the ΔE-E telescope at E = 2.2 MeV for the standard ^{4}He target and Ar post-stripper density (upper panel). The different components are labeled. The lower panel shows the background at the same energy measured only with the Ar post-stripper after removing the ^{4}He target gas. The running time for both spectra is the same.

are then counted in a ΔE-E telescope placed at the end of the beam line. The ratio between leaky ^{12}C events detected in the telescope and the number of ^{12}C projectiles is in the range of 4×10^{-11} at the high energy limit and 2×10^{-13} at the lower limit. Additionally, a beam suppression factor of the telescope alone of 10^{-3} —ratio of ^{16}O and leaky ^{12}C in the ΔE-E matrix (fig. 2)— can be achieved leading to a total suppression factor of better than 5×10^{-14}. ERNA is designed to study the reaction over the energy range E = 0.7 to 5.0 MeV. The detection of the ^{16}O recoils allows, for the first time, a direct measurement of the total cross-section of ^{12}C$(\alpha, \gamma)^{16}$O, including possible non-radiative transitions.

3 Experimental procedures

The number $N_{^{16}\mathrm{O}}$ of recoils collected in the telescope is given by the relation

$$N_{^{16}\mathrm{O}} = N_{^4\mathrm{He}} N_{^{12}\mathrm{C}} \sigma(E_{\mathrm{eff}}) T_{\mathrm{RMS}} \Phi_{\mathrm{R}} \epsilon \,, \qquad (1)$$

where $N_{^4\mathrm{He}}$ and $N_{^{12}\mathrm{C}}$ represent, respectively, the target number density and the number of projectiles impinging on the target, $\sigma(E_{\mathrm{eff}})$ is the cross-section at the effective interaction energy E_{eff}, T_{RMS} is the transmission of ERNA for the recoils in the selected charge state of probability Φ_{R}, and ϵ is the detection efficiency of the telescope. Therefore, $\sigma(E_{\mathrm{eff}})$ can be determined with high precision, if all quantities in eq. (1) are known with high accuracy.

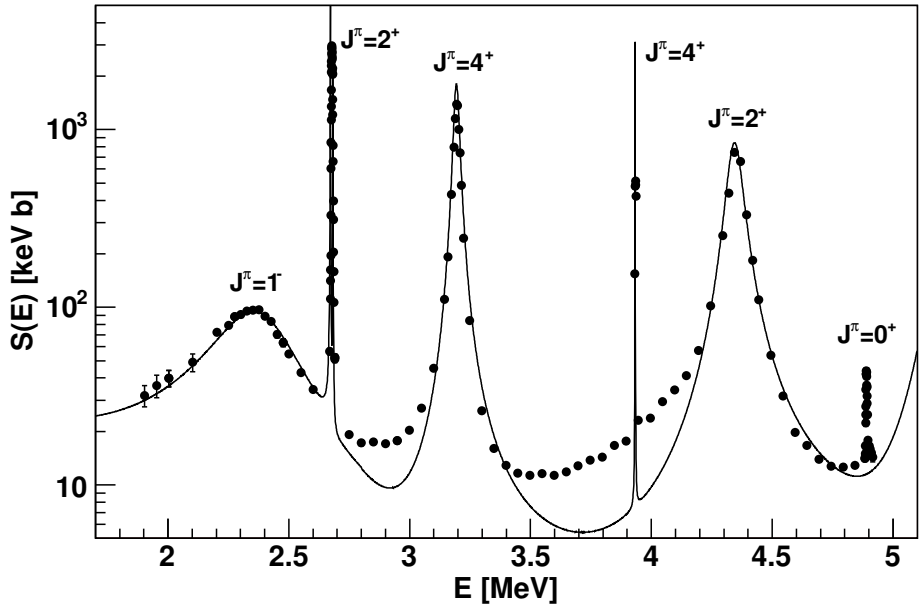

Fig. 3. Total $S(E)$ factor of the reaction $^{12}C(\alpha,\gamma)^{16}O$. Data near the narrow resonances at $E = 2.68, 3.9$, and 4.9 MeV are thick-target yields. The solid line represents the sum of the different amplitudes extracted from a recent R-matrix calculation [22]. Error bars shown are statistical only.

The thickness of the extended windowless He gas target was determined using the $^4He(^7Li,\gamma)^{11}B$ reaction at $E_{lab} = 1.668$ MeV [19], energy loss measurements of different ions [20], and the $^4He(^7Li,\ ^4He)^7Li^*$ reaction at $E_{lab} = 3.325$ MeV [21]. The weighted average of the results yields $N_{^4He} = 4.21 \pm 0.14 \times 10^{17}$ atoms/cm^2 with an effective target length of 42.6 ± 1.4 mm, that corresponds to an energy loss, E_{loss}, for the ^{12}C ions smaller than 25 keV in the investigated energy range. The small target thickness leads to a nearly constant cross-section along the target, thus $E_{eff} = (E_{beam} - E_{loss}/2)^* M_{^4He}/(M_{^{12}C} + M_{^4He})$.

The number of projectiles $N_{^{12}C}$ is determined through the detection of the elastically scattered ^4He nuclei in two collimated silicon detectors located in the target chamber at 75° from the beam axis. Calibration runs performed at each energy before and after the measurement runs allowed to relate the observed scattering rate to the concurrent beam current. The scattering rate was measured in short runs of typically 60 s to achieve a statistical precision of better than 1%. The beam current without target gas was monitored in a Faraday cup (FC2) located after the quadrupole triplet before and after the determination of the scattering rate. This procedure was found to be independent of the beam focussing and reproducible within the statistical error. A 100% transmission of the incident beam through the gas target is a requirement of the separator [19] and was verified by the full transmission through a retractable focussing aperture in front of the gas cell with a diameter of 3 mm.

The charge state distribution Φ_R of the ^{16}O recoils produced in the ^4He gas target depends on the geometric origin in the target: ^{16}O recoils produced in the upstream part of the target will most likely reach an equilibrium charge state distribution in the passage of the remaining target length, while those produced near the downstream end of the target will not, *i.e.* they will keep memory of the charge state at the moment of their formation. Since this effect is not accurately predictable [20], the charge state distribution of the ^{16}O recoils after passing the He gas is affected by a significant uncertainty. To remove this uncertainty, an Ar stripper was installed after the ^4He gas target with a number density $n_{Ar} = 5.6 \pm 0.6 \times 10^{16}$ atoms/cm^2. This density is sufficient for all ions produced at different locations in the ^4He target to reach the same charge state distribution. Finally, the observed ^{16}O charge state distribution in the combination of ^4He and Ar gas was measured over the full energy range [21]: for each charge state the separator was set properly and the resulting current observed at the end of the separator in FC4 (fig. 1). The measured charge state distribution differs from the equilibrium charge state distribution of ^{16}O ions in Ar gas [20] due to the effect of charge exchange in the ^4He rest gas in the downstream pumping stages of the gas target after the post-target stripper. This effect is energy and charge state dependent and amounts to a chance of the equilibrium charge state distribution of 20% at most.

The transmission of the separator T_{RMS} essentially depends on its acceptance compared to the emittance of the recoils, which, in turn, depends on γ-ray emission, target effects, and the beam emittance. The angular acceptance of ERNA has been measured using an ^{16}O beam and an electrostatic deflection unit [19], which can deflect the beam at any position within the target region in order to simulate the recoil ion angular opening at the different geometrical locations where ^{16}O recoils are produced. The energy acceptance was measured by varying the beam energy from the accelerator. For both quantities, ERNA

turned out to fulfill the requirements for measuring $\sigma(E_{\rm eff})$ in the energy range $E = 1.3$ to 5.0 MeV within a region of ± 70 mm around the target center, that includes 96% of the target nuclei. The angular straggling of the recoils in the gas target results in a loss of recoils less than 0.5%, which gives a final value of $T_{\rm RMS} = 1^{+0.0}_{-0.01}$ [21]. The detector efficiency $\epsilon_{\rm d} = 1$ is reduced by the transparency $T_{\rm PGAC}$ of the grids of a parallel grid avalanche counter at the entrance window of the ΔE-E telescope leading to a total detection efficiency $\epsilon = \epsilon_{\rm d} T_{\rm PGAC} = 0.980 \pm 0.005$.

It is important to note that the 100% transmission of the recoils in the selected charge state is a key requirement for measuring reliably the absolute capture cross-section $\sigma(E_{\rm eff})$ using a recoil mass separator. Indeed, this is a condition for determining $\sigma(E_{\rm eff})$ without a detailed knowledge of the distribution of the recoils in the phase space, which depends on the γ-ray energy and γ-ray angular distribution, on target effects and beam emittance.

Finally, background runs (fig. 2, lower panel) were performed at each energy using the Ar post-target stripper only. The measurements showed the presence of an ^{16}O background, where at energies above 2.0 MeV a signal-to-background ratio of typically 20 was observed. The observed background rate in the region of interest was normalized to the number of projectiles and subtracted at each energy. An investigation of this ^{16}O background excluded as possible sources a beam contamination, which is suppressed by the ERNA beam purification system, as well as elastic scattering on rest gas. There are strong indications that the background is mostly due to the fraction of the ^{12}C beam impinging on the plates of the first Wien filter, and possibly other beam line components, producing ^{16}O via ^{12}C + ^{12}C fusion, *e.g.* the ^{12}C(^{12}C, ^{8}Be)^{16}O reaction. Since the fraction of the beam impinging on the plates increases with decreasing energy, measurements at energies lower than $E = 2.0$ MeV are affected by a signal-to-background ratio significantly poorer than at higher energy.

Table 1. Astrophysical $S(E)$ factor of ^{12}C$(\alpha,\gamma)^{16}$O. The quoted errors are statistical only. The data in the energy range of the narrow resonances are left out.

E (MeV)	S (keV b)	E (MeV)	S (keV b)
1.903	31.8 ± 4.3	3.249	84.2 ± 2.5
1.953	36.3 ± 5.3	3.298	26.1 ± 0.9
2.003	39.9 ± 4.3	3.348	16.1 ± 0.5
2.102	49.0 ± 5.6	3.398	12.9 ± 0.5
2.202	72.3 ± 2.7	3.448	11.7 ± 0.4
2.252	79.1 ± 2.9	3.498	11.3 ± 0.4
2.277	88.4 ± 3.0	3.548	11.6 ± 0.4
2.302	90.9 ± 3.3	3.597	11.3 ± 0.4
2.327	95.1 ± 3.0	3.647	11.9 ± 0.3
2.352	96.4 ± 3.0	3.697	12.8 ± 0.4
2.376	96.7 ± 2.9	3.747	13.8 ± 0.4
2.402	88.8 ± 2.5	3.797	14.3 ± 0.4
2.426	83.0 ± 2.7	3.847	16.6 ± 0.5
2.451	70.2 ± 2.9	3.896	17.6 ± 0.5
2.476	63.3 ± 3.1	3.946	23.1 ± 0.7
2.476	63.3 ± 3.1	3.996	23.7 ± 0.7
2.501	54.7 ± 1.7	4.046	29.5 ± 0.9
2.551	42.8 ± 1.5	4.096	34.2 ± 1.0
2.601	34.4 ± 1.1	4.145	41.3 ± 1.1
2.750	19.2 ± 0.7	4.195	57.0 ± 1.7
2.800	17.3 ± 0.7	4.245	101.7 ± 2.1
2.850	17.4 ± 0.6	4.295	253.8 ± 4.1
2.900	17.1 ± 0.5	4.320	440 ± 11
2.949	17.7 ± 0.6	4.345	744 ± 11
2.999	20.3 ± 0.6	4.370	661 ± 13
3.049	27.0 ± 0.9	4.395	331.5 ± 5.5
3.099	45.3 ± 1.4	4.420	183.4 ± 4.9
3.144	110.6 ± 3.3	4.445	110.5 ± 2.5
3.158	191.9 ± 6.0	4.494	53.6 ± 1.6
3.174	432 ± 11	4.545	31.6 ± 0.9
3.184	797 ± 14	4.594	19.7 ± 0.6
3.189	1156 ± 21	4.644	16.7 ± 0.5
3.194	1392 ± 21	4.694	14.0 ± 0.4
3.199	1363 ± 13	4.744	12.7 ± 0.4
3.204	1001 ± 17	4.793	12.6 ± 0.4
3.209	740 ± 17	4.843	12.9 ± 0.4
3.214	484.6 ± 8.2	4.883	14.1 ± 0.4
3.224	244.5 ± 5.8	4.917	14.3 ± 0.8

4 Results and conclusions

Figure 3 and table 1 show the total $S(E)$ factor at $E = 1.9$ to 4.9 MeV obtained with ERNA; the statistical error is of the order of 4% or less at energies above 2.2 MeV and the systematic error is 6.5% (3% $N_{^4\rm He}$, 2% $N_{^{12}\rm C}$, 1% $T_{\rm RMS}$, 2% $\Phi_{\rm R}$, 0.5% ϵ). In fig. 3 we present also a comparison of our data with the sum of the different amplitudes as reported in [22], *i.e.* the ground-state transition ($E1$ and $E2$) plus cascade transitions. Note the good agreement in absolute $S(E)$ values between previous work and the present data on top of the $E = 2.4, 3.2$, and 4.3 MeV resonances. The R-matrix calculation represents the best fit to the available experimental data at that time including resonance information from [23]. One should note that in this analysis the interference effects of the cascade transitions are neglected. There is a clear disagreement at energies around $E = 3.0$ and 4.0 MeV, where the calculation of [22] underestimates the total cross-section, while it slightly overestimates the cross-section on the high-energy tail of the broad $J^\pi = 1^-$ resonance at $E = 2.4$ MeV.

A preliminary analysis indicates that these discrepancies may be partly caused by a wrong choice of the interference pattern of the different amplitudes, especially of the $E2$ amplitude. The analyses [22,24] show that the χ^2-fit is hardly sensitive to different $E2$ interference patterns leading to a broad range of extrapolated $S_{E2}(E_0)$ values. A detailed study of the influence of the present data on $S(E_0)$ is in progress, that requires an R-matrix code including a fit to the different amplitudes (see, for example, [15,22]) as well as to the total cross-section.

Finally, a new resonance was found in ^{12}C$(\alpha,\gamma)^{16}$O at $E = 4.888$ MeV, corresponding to a known 0^+ state ($\Gamma = 1.5 \pm 0.5$ keV) reported in [23]. The analysis of the recoil data results in a resonance strength $\omega\gamma = 11.2 \pm 1.5$ meV.

In conclusion, the ERNA approach provided new data of $^{12}C(\alpha,\gamma)^{16}O$ at energies above 1.9 MeV, which are needed for an improved $S(E_0)$ determination.

The authors thank the technical staff of the Mechanical Workshop and of the Dynamitron Tandem Laboratorium in Bochum for their support to the project. The project is supported in part by Deutsche Forschungsgemeinschaft (Ro429/35-2) and Istituto Nazionale di Fisica Nucleare (ERNA), and DAAD-CRUI VIGONI.

References

1. C. Rolfs, W.S. Rodney, *Cauldrons in the Cosmos* (University of Chicago Press, 1988).
2. G. Imbriani *et al.*, Astrophys. J. **558**, 903 (2001).
3. O. Straniero *et al.*, Astrophys. J. **583**, 878 (2003).
4. H.O.U. Fynbo *et al.*, Nature **433**, 136 (2005).
5. S. Woosley *et al.*, Nucl. Phys. A **718**, 3c (2003).
6. P. Dyer, C.A. Barnes, Nucl. Phys. A **233**, 495 (1974).
7. K.-U. Kettner *et al.*, Z. Phys. A **308**, 73 (1982).
8. A. Redder *et al.*, Nucl. Phys. A **462**, 385 (1987).
9. R.M. Kremer *et al.*, Phys. Rev. Lett. **60**, 1475 (1988).
10. J.M.L. Quellet *et al.*, Phys. Rev. C **54**, 1982 (1996).
11. G. Roters *et al.*, Eur. Phys. J. A **6**, 451 (1999).
12. D. Rogalla, Diploma Thesis (Ruhr-Universität Bochum, 1997).
13. L. Gialanella *et al.*, Eur. Phys. J. A **11**, 357 (2001).
14. R. Kunz *et al.*, Phys. Rev. Lett. **86**, 3244 (2001).
15. L. Buchmann *et al.*, Phys. Rev. C **54**, 393 (1996).
16. D. Rogalla *et al.*, Nucl. Instrum. Methods A **437**, 266 (1999).
17. D. Rogalla *et al.*, Eur. Phys. J. A **6**, 471 (1999).
18. D. Rogalla *et al.*, Nucl. Instrum. Methods A **513**, 573 (2003).
19. L. Gialanella *et al.*, Nucl. Instrum. Methods A **522**, 432 (2004).
20. D. Schürmann *et al.*, Nucl. Instrum. Methods A **531**, 428 (2004).
21. D. Schürmann *et al.*, to be published (2006).
22. R. Kunz *et al.*, Astrophys. J. **567**, 643 (2002).
23. D.R. Tilley, H.R. Weller, C.H. Cheves, Nucl. Phys. A **564**, 1 (1993).
24. R. Kunz, Thesis (Universität Stuttgart, 2002).